PRIMARY- AND SECONDARY-PARTICLE CONTRIBUTIONS TO THE DEPTH-DOSE DISTRIBUTION IN A PHANTOM SHIELDED FROM SOLAR-FLARE AND VAN ALLEN PROTONS*

R. T. Santoro, H. C. Claiborne, and R. G. Alsmiller, Jr.
Oak Ridge National Laboratory

Calculations have been made using the nucleon-meson transport code NMTC to estimate the absorbed-dose and dose-equivalent distributions in "astronauts" inside space vehicles bombarded by solar-flare and Van Allen protons. A spherical shell shield of specific radius and thickness with a 30-cm-diam. tissue ball at the geometric center was used to simulate the spacecraft-astronaut configuration. The absorbed dose and the dose equivalent from primary protons, secondary protons, heavy nuclei, charged pions, muons, photons, and positrons and electrons are given as a function of depth in the tissue phantom. Results are given for solar-flare protons with a characteristic rigidity of 100 MV and for Van Allen protons in a 240-nautical-mile circular orbit at 30° inclination angle incident on both 20-g/cm^2-thick aluminum and polyethylene spherical shell shields.

INTRODUCTION

In planning missions for manned space vehicles, it is necessary to have detailed information on the absorbed dose and dose equivalent received by the astronauts as a result of exposure to the natural radiation of space. This paper gives the results of calculations made with the nucleon-meson transport code NMTC (ref. 1) for the contributions of solar-flare and Van Allen protons to the dose distributions in a tissue phantom in a geometric model that simulates a "spacecraft-astronaut" configuration.

Calculational methods have been available for treating the transport of nucleons with energies below 400 MeV (ref. 2) for some time, but only approximate results (refs. 3-7) could be obtained for greater energies because of the lack of data on particle production from nucleon-nucleus and pion-nucleus collisions. Recently, however, calculated particle-production data for these interactions at high energies have been published (ref. 8). These data have been incorporated into the nucleon-meson transport code NMTC (ref. 1), and the results of calculations using NMTC have been shown to be in good agreement with experimental data for energies up to ∿3 GeV (refs. 9-11).

These improvements in the code permitted a more accurate representation of high-energy nucleon and pion transport and provide an accurate estimate of the contribution to the dose from charged pions and muons, as well as from the lepton component produced through muon decay. An estimate of the absorbed dose and dose equivalent from nucleons and charged mesons and their progeny was reported by Alsmiller *et al.* (ref. 12) for nucleons incident on tissue slabs. The results reported here give corresponding dose estimates for protons incident on a shielded spherical, tissue phantom.

In the following sections, the calculational methods and the spherical spacecraft-astronaut configuration are described. The incident proton spectra from both solar flares and the Van Allen belts are presented. A brief discussion of the transport calculation and the dose determinations are included. Finally, the results of the calculations are presented and discussed.

SPACECRAFT-ASTRONAUT CONFIGURATION

Depth-dose distributions were obtained for the geometric model shown in figure 1 that simulates a spacecraft-astronaut configuration. In this model, the spacecraft is considered to be a spherical shell having a fixed inner radius of 150 cm which gives a constant internal volume for all shell thicknesses. At the geometric center of the spacecraft is the astronaut who is represented by a 30-cm-diam. sphere of tissue. The composition of the tissue is shown in Table I.

TABLE I. COMPOSITION OF TISSUE

Element	Density of Nuclei (Nuclei/cm^3)
H	6.265×10^{22}
O	2.551×10^{22}
C	9.398×10^{21}
N	1.342×10^{21}

*Research funded by the National Aeronautics and Space Administration (Order H-38280A) under Union Carbide Corporation's contract with the U. S. Atomic Energy Commission.

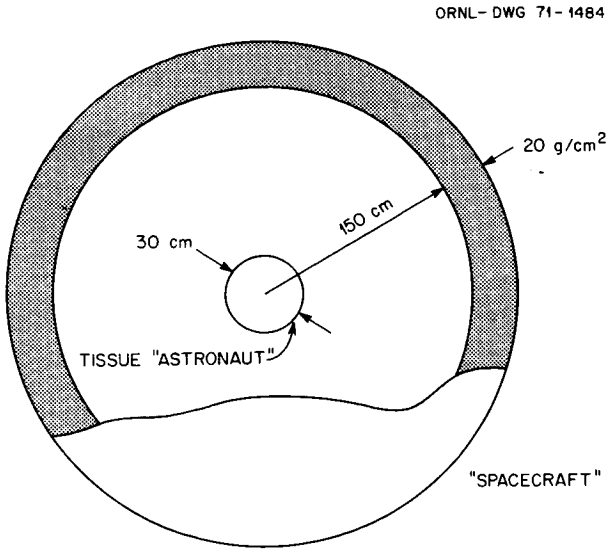

FIGURE 1. - A Schematic Diagram of the "Spacecraft-Astronaut" Configuration.

PROTON ENERGY SPECTRA

Solar-flare and Van Allen belt proton spectra are characterized by their nearly isotropic angular distributions and steep energy gradients. Since the intensity and energy spectrum vary markedly with altitude and geomagnetic coordinates in the Van Allen belts and from event to event for solar flares, it is essential in the shielding analysis of manned space flight missions that the representation of these spectra simulate those that might reasonably occur during a mission.

Solar Flares

At the higher particle energies, accurate solar-flare representations are realized when the time-integrated proton spectrum is expressed as an exponential function of magnetic rigidity; that is,

$$J(>E) = J_o \exp(- P(E)/P_o), \qquad (1)$$

where

$J(>E)$ is the omnidirectional fluence (p/cm^2) with kinetic energies above energy E,

$P(E)$ is the magnetic rigidity, and for protons $P(E) = (E^2 + 2M_p E)^{1/2}$,

M_p is the proton rest energy,

P_o is the characteristic rigidity of the flare,

J_o is an intensity parameter.

Differentiating equation 1 with respect to the kinetic energy, E, yields the differential kinetic energy spectrum

$$- \frac{dJ(>E)}{dE} = \frac{J_o}{P_o} \frac{(E+M_p)}{P(E)} \exp(- P(E)/P_o). \qquad (2)$$

The intensity is normalized such that

$$J_o = \frac{10^9}{\frac{1}{P_o} \int_{E_o}^{E_{max}} \frac{(E+M_p)}{P(E)} \exp(-P(E)/P_o) dE} \qquad (3)$$

where E_o is some lower cutoff energy in the spectrum.

Figure 2 is a plot of equation 2 for a flare of characteristic rigidity P_o = 100 MV and $J(>E_o)$ = 10^9 p/cm^2 in the energy range from 30 to 3000 MeV. The energy intervals and the values indicated designate the fraction of time that protons in the given energy interval were sampled for the transport calculations.

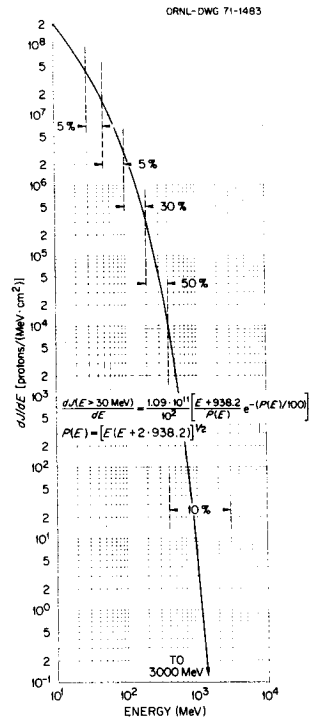

FIGURE 2. - A Solar-Flare Spectrum of Characteristic Rigidity P_o = 100 MV and Normalized to Contain 10^9 p/cm^2 With Kinetic Energy > 30 MeV.

Van Allen Belt

In the Van Allen belt, the average flux of protons above energy E that a spacecraft receives in orbit after time T is expressed by

$$J(>E) = T^{-1} \int_0^T J[(>E;B(t),L(t)]dt, \qquad (4)$$

where

$J[(>E;B(t),L(t)]$ represents the functional dependence of the omnidirectional flux above kinetic energy E in (B,L) coordinates and with time along the orbit path.

The omnidirectional flux can be approximately expressed by

$$J(>E;B,L) = J(>E_1;B,L) \times \exp[-(E - E_1)/E_o(B,L)], \qquad (5)$$

where

$J_o(>E_1;B,L)$ is the number of protons above an energy cutoff E_1, and

$E_o(B,L)$ is a fit parameter to the proton spectrum at each point in (B,L) space.

Equation 4 was solved by numerical integration using the computer code TRECO (ref. 13) developed by Vette and his coworkers (refs. 14-16), which utilizes previously determined flux maps and spectral fits of the Van Allen radiation field as input. In the code, the time dependence for J(>E;B,L) is obtained using Kepler's Laws to determine the geographic coordinates of an orbit as a function of time and transforming to the (B,L) system using a spherical harmonic expansion of the geomagnetic field. For the results given here, the AP7 flux map (ref. 16) and spectral parameters that give the best fit to the experimental data for proton energies >50 MeV were used to obtain the proton flux in the energy range $30 \leq E_p \leq 1000$ MeV. Use of this model for energies down to 30 MeV leads to a small overestimate of the flux in the 30- to 50-MeV range.

Figure 3 shows the proton flux for a 240-nautical-mile circular orbit obtained using TRECO (ref. 13) for orbit inclinations of 30°, 60°, and 90° to the equatorial plane. (At this altitude, negligible flux is obtained for a 0° orbit.) These data give the proton fluence averaged over an orbit time of one day. The larger values of the fluence observed for the 30° orbit arise from passage through the South Atlantic Anomaly. As in figure 2, the divisions on the energy scale and the values indicated between them represent the fraction of time that protons in the energy interval were sampled from in the transport calculation. The dose distributions presented in this paper were obtained using the 240-nautical-mile 30° orbit flux spectrum shown in figure 3.

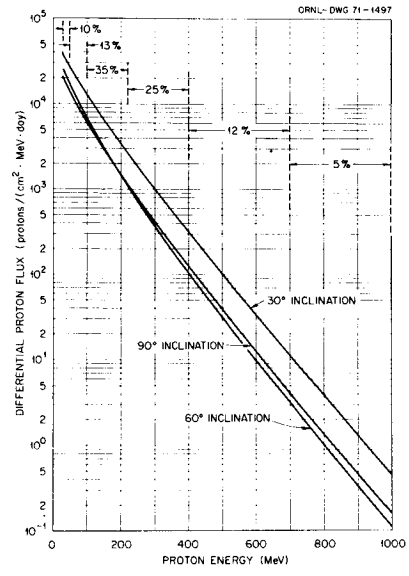

FIGURE 3. - Van Allen Belt Proton Spectra at a 240-Nautical-Mile Circular Orbit for Inclination Angles of 30°, 60°, and 90° to the Equatorial Plane. For the 30° orbit, the spectrum is normalized to contain 2.56×10^6 p/(cm^2 day) with kinetic energy > 30 MeV.

Method of Calculation

The details of the transport calculation are described by Coleman and Armstrong (ref. 1) and by Alsmiller *et al.* (ref. 12). For the results given here, the incident proton spectra were taken to be an omnidirectional fluence of 10^9 p/cm^2 for the solar flare and a time-averaged fluence of 2.56×10^6 p/(cm^2 day) for the Van Allen spectra having kinetic energy >30 MeV. The energy of the protons incident on the shield was determined by sampling from the spectrum according to the frequencies indicated in the energy bands shown in figures 2 and 3.

The incident protons, along with the secondary protons, neutrons, charged pions, and muons, were transported through the shield and tissue taking into account the energy and angular distributions of these particles. The energy loss in passage through the various media by means of excitation and ionization of the atomic electrons was treated in the continuous slowing-down approximation using known energy loss per unit distance for the charged particles (refs. 9 and 17). Heavy ions (mass > 1) were assumed to deposit all of their energy at their point of origin. Since the range of a heavy particle is short in all materials, this assumption is reasonably valid. The same assumption was made for electrons and positrons from muon decay and photons emitted through nonelastic nucleon-nucleus collisions and the decay of π° mesons. This assumption, though not entirely valid, is acceptable on the basis of the small contribution to the total dose by these particles.

For nucleons having energies >15 MeV and for pions above 2.2 MeV, the differential cross sections for nucleon and pion emission from nucleon-nucleus and pion-nucleus collisions were obtained from the intranuclear-cascade-evaporation model of nuclear reactions (refs. 8 and 18-20). This model gives the energy and angular distribution of the pions and nucleons emitted following a reaction, as well as an estimate of the energy of emitted deutrons, tritons, ^{3}He, alpha particles, and photons, and an approximate value of the kinetic energy of the recoiling residual nucleus from a nonelastic collision. The nucleon and pion nonelastic collision density was also obtained using this model. Except for capture of negative pions, proton-nucleus collisions below 15 MeV and pion-nucleus collisions below 2.2 MeV were ignored.

The intranuclear-cascade-evaporation model has been shown to be applicable at energies well below 50 MeV (ref. 21), and in all the calculations reported here the intranuclear-cascade-evaporation model was used to describe nucleon-nucleus collisions at energies >15 MeV, and the evaporation model was used to describe particle production from neutron-nucleus nonelastic collisions at energies below 15 MeV. Particles resulting from neutron-nucleus nonelastic collisions below 15 MeV were obtained using the evaporation code EVAP-4 (ref. 20) in conjunction with the total nonelastic cross-section data on the 05R master cross-section tape.*

In these calculations, the absorbed dose and the dose equivalent were computed as a function of depth in the simulated tissue astronaut. In computing the dose equivalent, the quality factor was taken to be a function of linear energy transfer. For protons, the LET curve (ref. 23) based on the recommendations of the National Committee on Radiation Protection and Measurement was used. For charged pions and muons, the quality factor as a function of LET was taken to be the same as that for protons, and the quality factor vs LET curve was constructed in a manner similar to the proton curves as described in ref. 23. A quality factor of 20 was assigned to the energy deposited by all heavy nuclei. For electrons, positrons, and photons a quality factor of unity was used.

DISCUSSION OF RESULTS

Calculations to estimate the absorbed dose and dose equivalent as a function of depth in the tissue have been carried out for solar flare and Van Allen protons incident on 20-g/cm^2-thick aluminum and polyethylene shields. The incident spectrum for solar-flare protons is given in figure 2 and the incident Van Allen proton spectrum for an altitude of 240 nautical miles at a 30° inclination to the equator is shown in figure 3. The depth-dose distributions presented here are normalized to an isotropic incident fluence of 10^9 p/cm^2 for the flare data and to a time-averaged fluence of 2.56×10^6 p/(cm^2 day) for the Van Allen protons.

Figure 4 gives the contributions to the absorbed dose when solar-flare protons are incident on the 20-g/cm^2-thick aluminum shield. The largest contribution to the dose arises from primary protons, that is, protons which have not suffered any nuclear interactions in the shield or tissue. For these protons, the dose is due entirely to excitation and ionization of atomic electrons in the tis-

*The master cross-section tape for use in the 05R Monte Carlo code (ref. 22) is available on request from the Radiation Shielding Information Center, Oak Ridge National Laboratory, Oak Ridge, Tenn. 37830

sue. The histogram labeled "secondary protons" gives the absorbed dose from the excitation and ionization of atomic electrons by protons produced by nonelastic nucleon- and pion-nucleus collisions in the shield and the tissue and from the elastic collisions of nucleons and pions with hydrogen nuclei in the tissue. The histogram labeled "heavy nuclei" gives the absorbed dose from particles with mass number greater than unity produced from nonelastic nucleon-nucleus and pion-nucleus collisions, from recoiling nuclei from elastic neutron-nucleus collisions, and from nonelastic nucleon-nucleus and pion-nucleus collisions. The histogram labeled "charged pions" gives the absorbed dose from the excitation and ionization of atomic electrons by both positively and negatively charged pions produced from nucleon-nucleus and pion-nucleus collisions. The histogram labeled "photons from neutral pions" gives the absorbed dose produced by the photons arising from the decay of neutral pions. (The assumption was made that photons were absorbed at the point of origin.) The histogram labeled "electrons, positrons, and photons" gives the absorbed dose from electrons and positrons produced by muon decay, and the absorbed dose from the photons produced by nucleon-nucleus and pion-nucleus nonelastic collisions. The histogram labeled "muons" gives the absorbed dose from the excitation and ionization of atomic electrons by both positively and negatively charged muons.

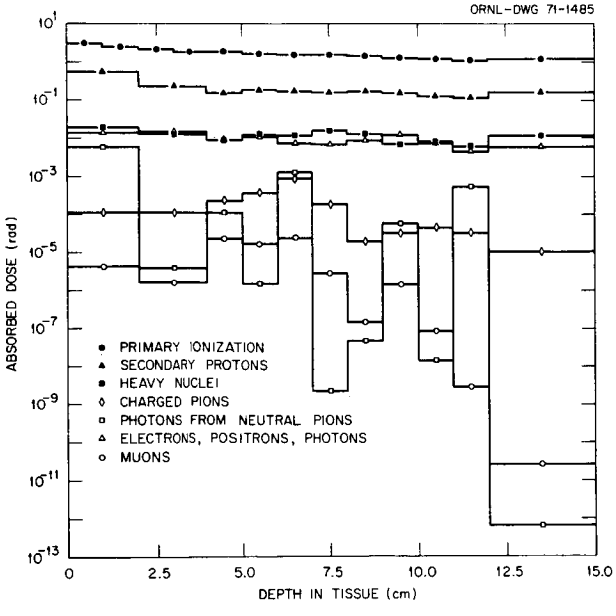

FIGURE 4. - Absorbed Dose for Various Particles Vs Depth in Tissue for P_o = 100 MV Solar-Flare Protons Isotropically Incident on a 20-g/cm^2-thick Aluminum Spherical Shell Shield.

The absorbed dose from primary-proton ionization is given as the average over each depth interval (1 cm) except for the central region of the tissue ball when the value is the average over 3 cm. For all secondary-particle contributions to the absorbed dose, the results are given as an average over the first two-centimeter and second two-centimeter depth intervals in the tissue. The remaining intervals are presented in the same manner as for the primary dose contribution.

Figure 5 shows the dose-equivalent distributions from the various particles for the solar-flare protons in the 20-g/cm^2-thick aluminum spherical shell shield. It should be noted that the dose equivalents for secondary protons and heavy nuclei are comparable (within a factor of $\sim$2). The increased contribution to the dose-equivalent results from the large quality factor (20) associated with these particles.

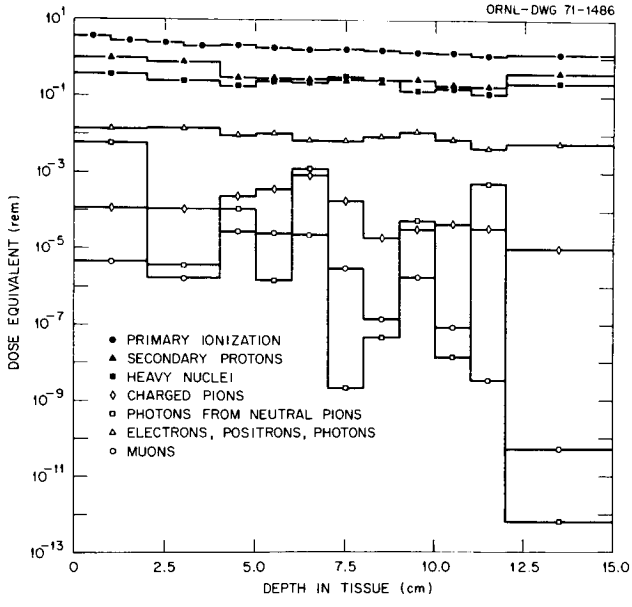

FIGURE 5. - Dose Equivalent for Various Particles Vs Depth in Tissue for P_o = 100 MV Solar-Flare Protons Isotropically Incident on a 20-g/cm^2-thick Aluminum Spherical Shell Shield.

Figures 6 and 7 show the absorbed dose and dose-equivalent distributions, respectively, from the various kinds of particles produced when the P_o = 100 MV solar flare is incident on a 20-g/cm^2-thick polyethylene spherical shell shield. Figures 8 and 9 are the absorbed dose and dose-equivalent distributions, respectively, due to primary-proton ionization and the total secondary-particle contribution to the dose for the aluminum and polyethylene spherical shell shields for the incident flare protons. These data indicate the reduction in the absorbed dose and dose equivalent realized using a polyethylene shield. This reduction is due primarily to the increased differential stopping power vs proton energy associated with polyethylene. The reduction in dose is gained at the expense of increased linear dimensions because of the additional thickness of the polyethylene shield (∿3).

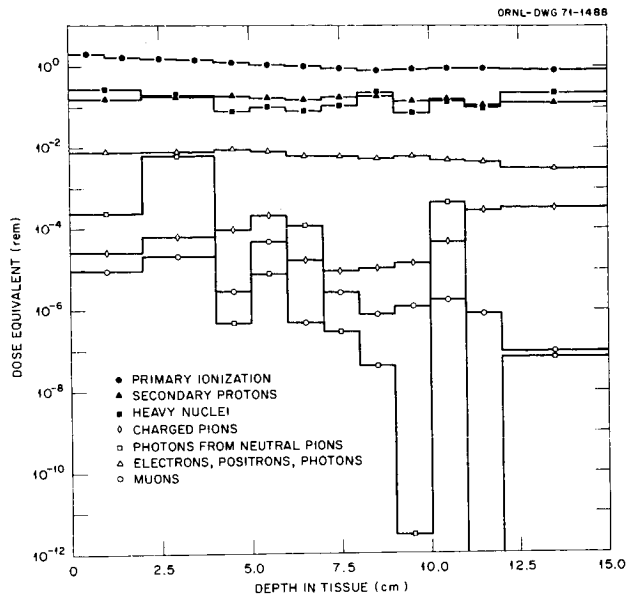

FIGURE 7. - Dose Equivalent for Various Particles Vs Depth in Tissue for P_o = 100 MV Solar-Flare Protons Isotropically Incident on a 20-g/cm^2-thick Polyethylene Spherical Shell Shield.

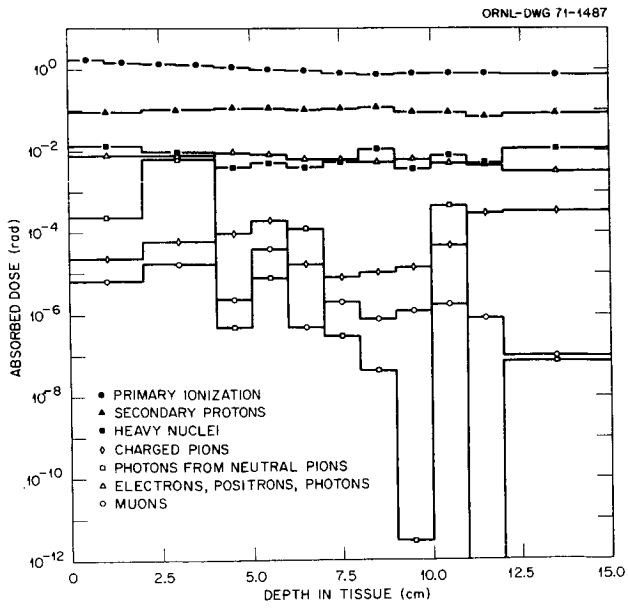

FIGURE 6. - Absorbed Dose for Various Particles Vs Depth in Tissue for P_o = 100 MV Solar-Flare Protons Isotropically Incident on a 20-g/cm^2-thick Polyethylene Spherical Shell Shield.

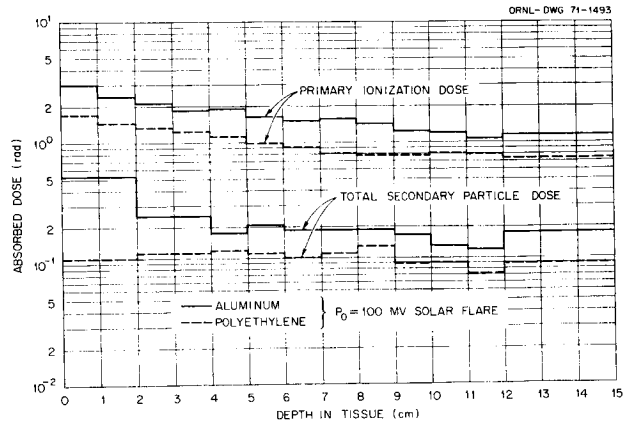

FIGURE 8. - Comparison of the Absorbed Dose Vs Depth in Tissue From the Primary-Proton Ionization and the Secondary Particles for Solar-Flare Protons (P_o = 100 MV) Isotropically Incident on 20-g/cm^2-thick Aluminum and Polyethylene Spherical Shell Shields.

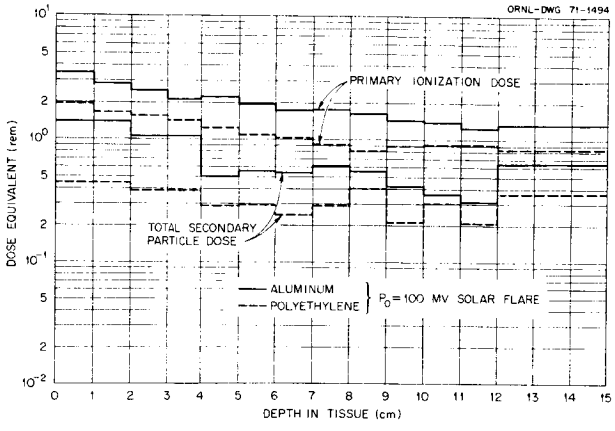

FIGURE 9. - Comparison of the Dose Equivalent Vs Depth in Tissue from the Primary-Proton Ionization and the Secondary Particles for Solar-Flare Protons (P_0 = 100 MV) Isotropically Incident on 20-g/cm^2-thick Aluminum and Polyethylene Spherical Shell Shields.

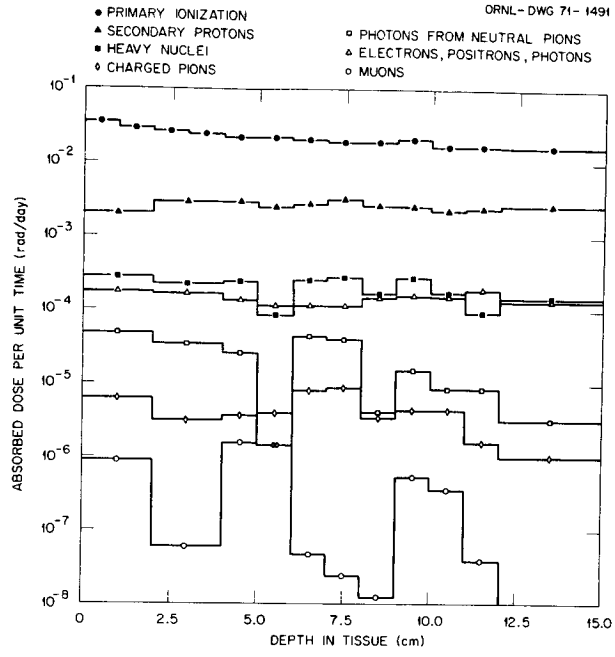

FIGURE 10. - Absorbed Dose for Various Particles Vs Depth in Tissue for Van Allen Protons (240-Nautical-Mile Circular Orbit at 30° Inclination) Isotropically Incident on a 20-g/cm^2-thick Aluminum Spherical Shell Shield.

Figures 10 and 11 show the absorbed dose and dose-equivalent distributions, respectively, vs depth in the tissue when Van Allen protons are incident on the 20-g/cm^2-thick aluminum spherical shell shield. As for the incident solar-flare protons, the principal contribution to the dose distributions is from primary-proton ionization. The dose component from secondary protons created in the shield, as well as the tissue, is down approximately one order of magnitude. In figure 11, the dose equivalent from secondary protons and heavy nuclei are comparable. The large value of the dose equivalent from the heavy nuclei component is caused by the large (20) quality factor associated with these particles.

Figures 12 and 13 give the absorbed dose and dose-equivalent distributions, respectively, vs depth in the tissue when the Van Allen protons are incident on the 20-g/cm^2-thick polyethylene shield. As in all the previous results, the largest contribution to the dose is due to the primary proton ionization.

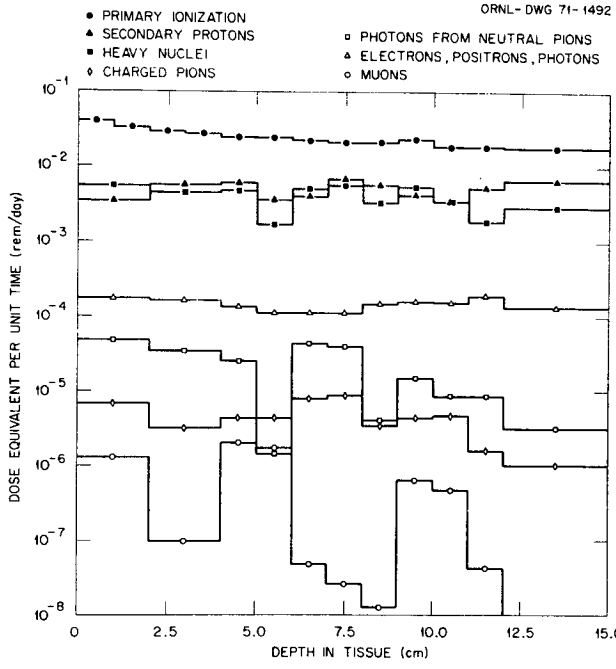

FIGURE 11. - Dose Equivalent for Various Particles Vs Depth in Tissue for Van Allen Protons (240-Nautical-Mile Circular Orbit at 30° Inclination) Isotropically Incident on a 20-g/cm^2-thick Aluminum Spherical Shell Shield.

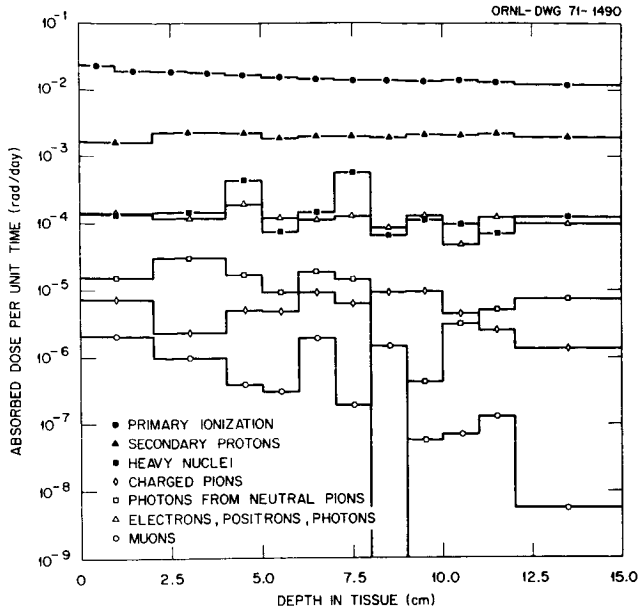

FIGURE 12. - Absorbed Dose for Various Particles Vs Depth in Tissue for Van Allen Protons (240-Nautical-Mile Circular Orbit at 30° Inclination) Isotropically Incident on a 20-g/cm^2-thick Polyethylene Spherical Shell Shield.

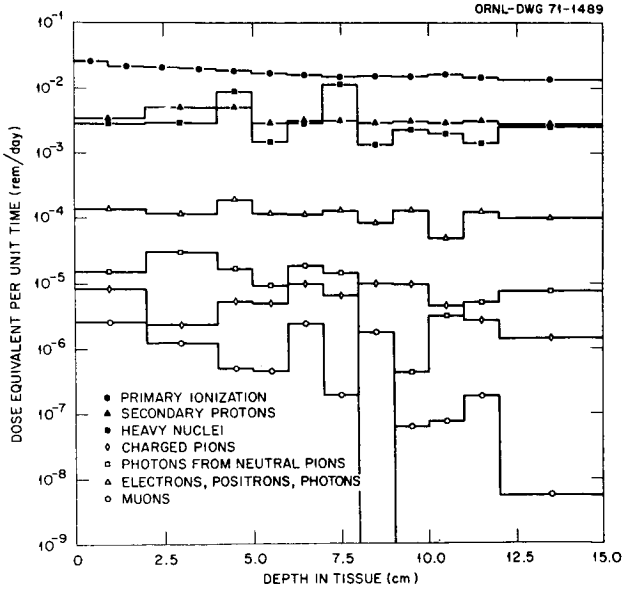

FIGURE 13. - Dose Equivalent for Various Particles Vs Depth in Tissue for Van Allen Protons (240-Nautical-Mile Circular Orbit at 30° Inclination) Isotropically Incident on a 20-g/cm^2-thick Polyethylene Spherical Shell Shield.

Figures 14 and 15, which are based on the results of figures 12 and 13, compare the primary ionization dose and the total secondary-particle dose contributions to the absorbed dose and dose equivalent, respectively. The reduced dose achieved with the polyethylene shield is from the larger differential stopping power of polyethylene compared to aluminum.

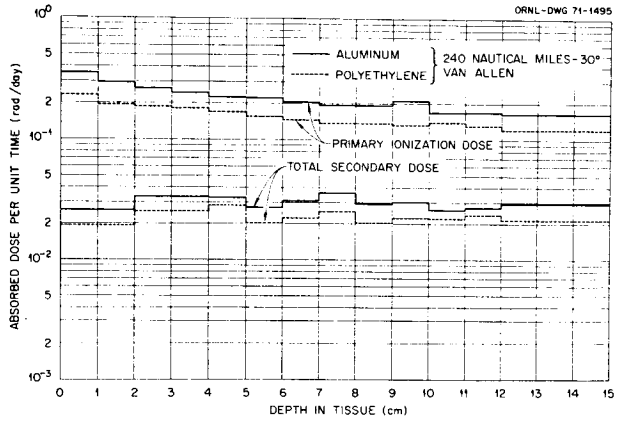

FIGURE 14. - Comparison of the Absorbed Dose Vs Depth in Tissue from the Primary-Proton Ionization and Secondary Particles for Van Allen Protons Isotropically Incident on 20-g/cm^2-thick Aluminum and Polyethylene Spherical Shell Shields.

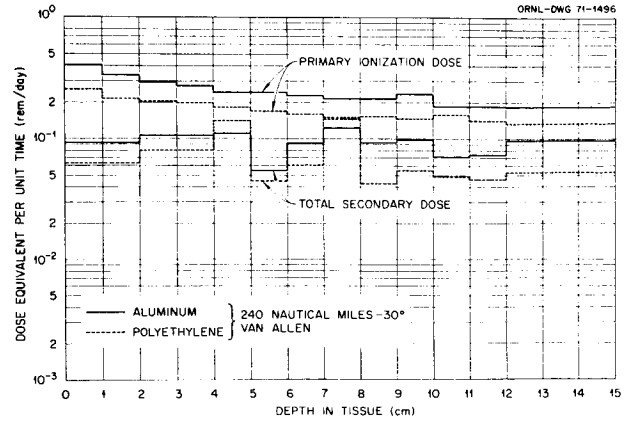

FIGURE 15. - Comparison of the Dose Equivalent Vs Depth in Tissue from the Primary-Proton Ionization and Secondary Particles for Van Allen Protons Isotropically Incident on 20-g/cm^2-thick Aluminum and Polyethylene Spherical Shell Shields.

The absorbed dose and dose-equivalent results reported here indicate clearly that for thin shields ($\lesssim$20 g/cm^2) the principal contribution to the dose from solar-flare protons in the energy range from 30 to 3000 MeV and Van Allen protons in the energy range from 30 to 1000 MeV is due to primary-proton ionization. Up to $\sim$10% of the total absorbed dose is due to secondary protons. The contributions to the absorbed dose from electrons, positrons, and photons compare with that due to heavy nuclei and are approximately two orders of magnitude lower than the primary-proton dose. The contribution to the dose equivalent from heavy nuclei is comparable to that of secondary protons. However, the contributions to the absorbed dose and dose equivalent from charged pions, photons from the decay of neutral pions, and muons are small compared to the primary-particle dose. The fluctuations in the distributions arise from generally poor statistics.

ACKNOWLEDGMENT

The authors wish to thank Dr. T. W. Armstrong for his comments and suggestions on the details of the transport calculation and analysis of these data.

REFERENCES

1. COLEMAN, W.A.; and ARMSTRONG, T.W.: The Nucleon-Meson Transport Code NMTC. Oak Ridge National Laboratory Document ORNL-4606, 1970.
2. KINNEY, W.E.: The Nucleon Transport Code, NTC. Oak Ridge National Laboratory Document ORNL-3610, 1964.
3. WRIGHT, H.A., et al.: Health Phys. Vol. 16, 1969, p. 13.
4. SNYDER, W.S., et al.: Nucl. App. Vol. 6, 1969, p. 336.
5. NEUFELD, JACOB, et al.: Health Phys. Vol. 17, 1969, p. 449.
6. ALSMILLER, R.G., JR.: Nucl. Sci. Eng. Vol. 27, 1967, p. 158.
7. SCOTT, W. WAYNE; and ALSMILLER, R.G., JR.: Comparisons of Results Obtained with Several Proton Penetration Codes. Oak Ridge National Laboratory Document ORNL-RSIC-17, 1967.
8. BERTINI, H.W.: Phys. Rev. Vol. 188, p. 1711.
9. COLEMAN, W.A.; and ALSMILLER, R.G., JR.: Nucl. Sci. Eng. Vol. 34, 1968, p. 104.
10. ARMSTRONG, T.W.; and ALSMILLER, R.G., JR.: Nucl. Sci. Eng. Vol. 33, 1968, p. 291.
11. ARMSTRONG, T.W.: J. Geophys. Res. Vol. 74, 1969, p. 1361.
12. ALSMILLER, R.G., JR.; ARMSTRONG, T.W.; and COLEMAN, W.A.: Nucl. Sci. Eng. Vol. 42, 1970, p. 367.
13. Data User's Note: TRECO, An Orbital Integration Computer Program for Trapped Radiation. National Space Science Data Center, Goddard Space Flight Center, NASA, Document NSSDC-68-02, 1968.
14. VETTE, J.I.: Models of the Trapped Radiation Environment, Volume I: Inner Zone Protons and Electrons, NASA Document SP-3024, 1966.
15. KING, J.H.: Models of the Trapped Radiation Environment, Volume IV: Low Energy Protons, NASA Document SP-3024, 1967.
16. LAVINE, J.P.; and VETTE, J.I.: Models of the Trapped Radiation Environment, Volume V: Inner Belt Protons. NASA Document SP-3024, 1969.
17. BETHE, H.; and ASHKIN, J.: Passage of Radiation Through Matter, p. 166 in Experimental Nuclear Physics, E. Segre, ed., Part II. John Wiley & Sons, New York, 1963.
18. BERTINI, H.W.: Nucl. Phys. Vol. 87, 1966, p. 138.
19. BERTINI, H.W.: Phys. Rev. Vol. 131, 1963, p. 1801; with erratum Phys. Rev. Vol. 138, 1965, AB2.
20. GUTHRIE, M.P.: EVAP-4: Another Modification of a Code to Calculate Particle Evaporation from Excited Compound Nuclei. Oak Ridge National Laboratory Document ORNL-TM-3119, 1970.
21. ALSMILLER, R.G., JR.; and HERMANN, O.W.: Nucl. Sci. Eng. Vol. 40, 1970, p. 254,
22. IRVING, D.C., et al: 05R, A General Purpose Monte Carlo Neutron Transport Code. Oak Ridge National Laboratory Document ORNL-3622, 1965.
23. TURNER, J.E., et al.: Health Phys. Vol. 10, 1964, p. 783.